Materials Transactions, Vol. 47, No. 11 (2006) pp. 2711 to 2717
Special Issue on Advances in Computational Materials Science and Engineering IV
©2006 The Japan Institute of Metals

Molecular Dynamics Simulation of Grain Boundary Formation and Migration in Silicon

Kenjiro Sugio*, Hiroshi Fukushima and Osamu Yanagisawa

Mechanical System Engineering, Graduate School of Engineering, Hiroshima University, Higashi-Hiroshima 739-8527, Japan

Molecular dynamics simulation using Tersoff potential was carried out to investigate the formation and the migration of (010) Σ5 twist boundary in silicon. Effects of carbon atoms on the grain boundary formation and the grain boundary migration were also investigated. Amorphous thin layers remained at the twist boundary even after crystallization, and changes in the thickness of this layers caused grain boundary migration. When carbon atoms were segregated at the twist boundary, these atoms prevented shrinkage of an amorphous thin layer, and the grain boundary migration was retarded. Precipitated carbon atoms within the grain produces a strain field and this strain field possibly became driving force for the grain boundary migration. [doi:10.2320/matertrans.47.2711]

(Received May 23, 2006; Accepted August 1, 2006; Published November 15, 2006)

Keywords: *molecular dynamics simulation, grain boundary formation, grain boundary migration, silicon, carbon*

1. Introduction

Polycrystalline silicon (poly-Si) is used for solar cells[1] and thin-film transistors,[2] and is also a candidate structural material in micro-electro-mechanical systems.[3] Grain Boundaries (GB's) affect the electrical and mechanical properties of poly-Si, and understanding of GB's provides improvements in the properties of poly-Si. GB's observed in poly-Si are roughly classified into a twin boundary and a random GB. Experimental results showed that twin boundaries were electrically inactive,[4] and it is thought that twin boundaries do not affect the electrical property of poly-Si. In contrast, random GB's are thought to deteriorate the electrical and mechanical properties of poly-Si, since dangling-bonds are possibly formed at these boundaries. Although the fraction of random GB's observed in poly-Si is less than that of twin boundaries,[5,6] random GB's strongly affect the properties of poly-Si.[7]

Computational studies of coincidence twist boundaries in Si have been conducted,[8,9] since atmistic structure of these boundaries contain large bond distortions and features of these boundaries are similar to random GB's. Keblinski *et al.* carried out Molecular Dynamics (MD) simulation of coincidence twist boundaries[9] and random GB's[10] in Si using Stllinger and Weber potential.[11] They reported that both of these boundaries formed of amorphous layers. These previous computer simulation studies focused on the determination of the most stable configuration of coincidence twist boundaries and random GB's. However, the atomistic processes of the GB formation during crystallization and GB migration have not been investigated. The grain structure of poly-Si can be changed during subsequent annealing,[12] and understanding of the GB migration is also important.

Although a great progress has been achieved in ab initio computer simulation work for the atomic-scale studies, it is still difficult to apply this method to the long-period and large-scale simulation. Therefore, various empirical interatomic potentials for Si have been proposed.[11,13] Tersoff potential[14–16] is one of these potentials. Although the melting point estimated by Tersoff potential is higher than the actual melting point, it can well reproduce the structure of amorphous Si[17] and liquid Si.[18] The calculated activation energy of Si solid-phase epitaxy using the potential agrees well with the experimental value.[19]

In the present study, we have carried out Langevin[20] MD simulations using Tersoff potential[16] to investigate the formation of a GB during crystallization. The atomistic processes of the GB formation and the GB migration have been also investigated.

2. Simulation Procedure

Motion of atoms was analyzed by solving Langevin equation to maintain a constant temperature.[20] The equation of motion for atoms is

$$m\frac{dv_i}{dt} = F_i(t) - m\gamma v_i + R_i(t), \tag{1}$$

where m is the atomic mass, $\boldsymbol{v}_i$ is the velocity of the atom i, $\boldsymbol{F}_i(t)$ is the internal force calculated by Tersoff potential, γ is the viscosity, and $\boldsymbol{R}_i(t)$ is the random force acting on the atom i. The viscosity γ was set at $5\,\mathrm{ps}^{-1}$, and the random force was generated by a random number sequence. A random number sequence for each MD simulation did not change throughout the simulation. The generalized Runge-Kutta method for a stochastic differential equation[21] was applied to integrate the equations, and the time step for the integration was 1.0×10^{-3} ps. Periodic boundary condition was applied to the simulation cell. The size of cell did not change throughout the simulation. Conjugate Gradient (CG) method[22] was applied to minimize the total energy of the simulation cell after each MD simulation.

Figure 1(a) shows the original simulation cell that contains (010) Σ5 twist boundary. The atom positions in the cell are defined with Cartesian coordinates. The left side crystal has edges of ⟨100⟩ directions that are parallel to x, y and z directions. The right side crystal has the same structure as that of the left side crystal but is rotated clockwise 36.9

*Corresponding author, E-mail: ksugio@hiroshima-u.ac.jp

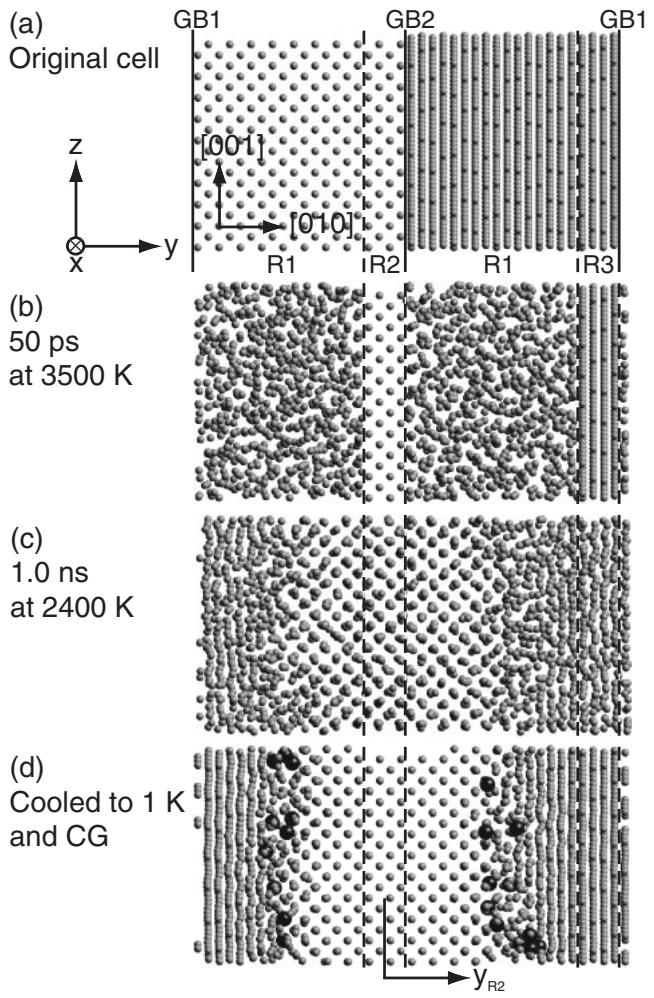

Fig. 1 Snapshots of the y-z projection of atoms during MD simulation. (a) The original simulation cell contains (010) Σ5 twist boundary. The right side crystal is made by rotating clockwise the left side crystal 36.9 degrees around the y-axis. GB1 and GB2 indicate grain boundaries, and details of R1 and R2 are explained in the text. (b) After R1 was melted at 3500 K for 50 ps. (c) After quench and 1 ns at 2400 K. (d) After CG method. Small gray spheres are atoms having coordination number 4, and large black spheres are the rest of atoms having 3, 5, 6 and 7 coordination numbers.

degrees around the y-axis. Two (010) Σ5 twist boundaries (GB1 and GB2) are introduced in the cell because of the periodic boundary condition. Two thousands atoms are included in the cell whose size is $5a_0 \times 10a_0 \times 5a_0$ (a_0: lattice constant), where a_0 was set at 0.543 nm. The cell was divided into three parts (R1, R2 and R3). R1 was melted, and R2 and R3 were used as seeds for crystallization.

Figure 2 shows the heat treatment used for MD simulation of the present twist boundary. R1 was first kept at 3500 K for 50 ps to make liquid phase and then R1 was quenched to crystallization temperature at the cooling rate of 1.0×10^{14} deg·s^{-1}. Cook and Clancy[23] reported that the calculated melting point (T_m) of Si was 2547 K using Tersoff potential. Our simulation showed melting of the seed R2 and R3 at 2500 K (0.98 T_m), and six crystallization temperatures, 1900 K (0.75 T_m), 2000 K (0.79 T_m), 2100 K (0.82 T_m), 2200 K (0.86 T_m), 2300 K (0.90 T_m) and 2400 K (0.94 T_m), were chosen. Then, fixed atoms in R2 were released and the

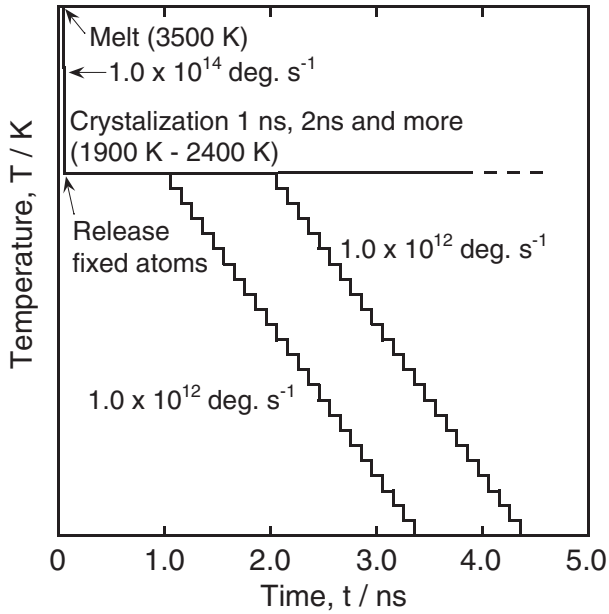

Fig. 2 Schematic presentation of the heat treatments used for the present MD simulation of the (010) Σ5 twist boundary.

whole cell was kept at a crystallization temperature for 1 and 2 ns. Two crystallization periods of 1 and 2 ns were chosen for the present twist boundary. Finally, the cell was cooled to 1 K at the cooling rate of 1.0×10^{12} deg·s^{-1}, where a temperature was lowered stepwise 100 degrees after every 0.1 ns.

3. Results and Discussion

3.1 Formation of GB's

Figs. 1(b), (c) and (d) show the typical snapshots of the y-z projection of atoms during a MD simulation. Fig. 1(b) corresponds to the snapshot just after 50 ps heating at 3500 K, and the melting of R1 is observed. Then, the cell was quenched and kept at 2400 K for 1.0 ns, and the result is shown in Fig. 1(c). Nearly all the part of R1 was crystallized and a new GB was formed between R2 and R3. Finally, the cell was cooled to 1 K and the total energy of the cell was minimized by CG method. Non-crystallized thin layers remained in the GB region as shown in Fig. 1(d). The coordination number was estimated by counting neighbor atoms within the cut-off distance of Tersoff potential. Small gray spheres are silicon atoms having coordination number 4, and large black spheres are silicon atoms having 3, 5, 6 and 7 coordination numbers. Large black spheres are observed in the GB region and are not observed in the crystalline part of the cell. This means that defects such as interstitials and vacancies were not introduced in the crystalline part of the cell.

The parallel translation of the whole cell happened in the present simulation. Random forces in Langevin equation (1) caused Brownian motion of the whole cell. Some atoms in R2 must be fixed during MD simulation to prevent this motion. However, the fixed atoms prevent the movement of seed-crystal R2 in the liquid, and this procedure has a possibility that GB structures are not optimized sufficiently. Therefore,

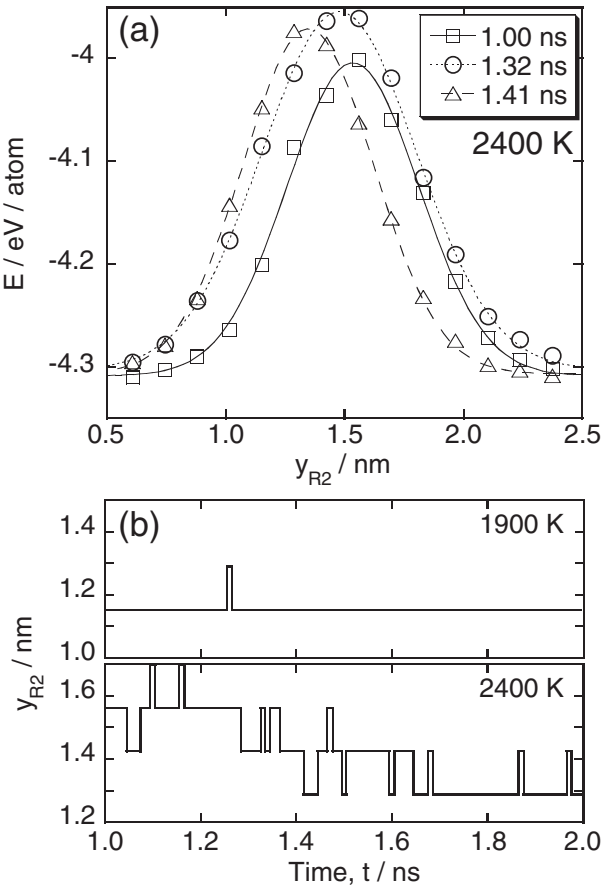

Fig. 3 (a) Three typical potential energy profiles after 1.0, 1.32 and 1.41 ns at 2400 K. The definition of y_{R2} is explained in the text. (b) The peak position of the potential energy profile versus time at 1900 and 2400 K.

the present MD simulation was carried out without fixing atoms in R2. We thought that Brownian motion of the whole cell did not affect the process of crystallization and GB formation. In Figs. 1(b), (c) and (d), a seed crystal was adjusted to the initial position.

3.2 Migration of GB's

In order to investigate the mechanism of GB migration, potential energy profiles along the y direction were evaluated during MD simulation after crystallization. Compression pressure ($\sigma_{xx}, \sigma_{yy}, \sigma_{zz}$) was applied to the simulation cell after crystallization because the size of cell did not change throughout the simulation. At 2400 K, σ_{xx}, σ_{yy} and σ_{zz} was about 3.0, 3.2 and 3.0 GPa, respectively. Figure 3(a) shows the three typical potential energy profiles for the GB migration at 2400 K. The horizontal axis y_{R2} is the distance from the center of R2 and the definition of y_{R2} is shown in Fig. 1(d). The vertical axis E is the average energy per atom in (010) slices of 0.25 a_0 thickness, where energies of atoms were averaged for 10 ps. Average energy per atom after 1.0, 1.32 and 1.41 ns at 2400 K are plotted in the figure, and curves show the results of Gaussian fitting of the plotted energies. The Full Width at Half Maximum (FWHM) was 0.65 nm at 1.0 ns, and the width of the non-crystallized thin layer was estimated to be about 1.25 a_0. The FWHM increased to 0.77 nm at 1.32 ns. This means that thickness of the non-crystallized thin layer expanded, and the expanded width was about 0.25 a_0. Then, the FWHM decreased to 0.65 nm at 1.41 ns. The peak position shifted and the FWHM approached to that at 1.0 ns. These changes in potential energy profiles suggest that the GB migration is caused by expansion and shrinkage of the non-crystallized thin layer.

Figure 3(b) shows the peak position of potential energy profiles at 1900 and 2400 K as a function of time. Since non-crystallized thin layers remained at the GB region, it is difficult to determine the position of the GB. Therefore, we considered the peak position as the position of the GB. The peak position shifted during MD simulation at 2400 K for 1.0 ns, which means that the GB migrated. In contrast, the peak position did not shift during MD simulation at 1900 K for 1.0 ns.

Driving force for GB migration is not applied in the present simulation model, and the peak position fluctuated by expansion and shrinkage of the non-crystallized thin layer. If driving force for GB migration is applied, the peak position will shift in one direction. Fluctuations observed in Fig. 3(b) suggest that (010) $\Sigma5$ twist boundary is unstable. The grain boundary populations in poly-Si were investigated experimentally.[5,6] The fraction of coincidence twist boundaries and random GB's was considerably less than that of twin boundaries. These experimental results suggest that coincidence twist boundaries is unstable.

3.3 GB energies

After the heat treatments shown in Fig. 2, total energy of the cell was minimized by CG method and GB energies were calculated by

$$E_{GB} = (E_{total}[N] - NE_{coh})/S_{GB}, \tag{2}$$

where $E_{total}[N]$ is the total energy of the simulated cell, N is the number of atoms in the cell, E_{coh} is the cohesive energy of Si crystal and S_{GB} is the total GB area. Figure 4 shows GB energies for each crystallization temperature. MD simulation of two crystallization periods (1 ns and 2 ns) was carried out at six crystallization temperatures (1900, 2000, 2100, 2200, 2300 and 2400 K). Moreover, three different calculations were carried out for each condition of MD simulation, changing random number sequences. Six GB energies were evaluated for each condition, because the cell had two GB's (GB1 and GB2). The open symbols in the figure represent respective GB energies and closed symbols represent the average of six GB energies. Seventy-two GB energies were obtained after all, and the average of seventy-two GB energies was 1272 mJ m^{-2}. The highest GB energy, 1495 mJ m^{-2}, was obtained by the heat treatment of 1 ns crystallization at 1900 K. The lowest GB energy, 1143 mJ m^{-2}, was obtained by the heat treatment of 1 ns crystallization at 2100 K. The GB energy in the original cell shown in Fig. 1(a) was 1718 mJ m^{-2} using CG method. Therefore, the GB energies were reduced after the heat treatments because of the formation of non-crystallized thin layers at GB's.

Keblinski *et al.*[9] carried out MD simulation for the four types of twist boundaries in Si such as (010) $\Sigma29$, (010) $\Sigma17$, (110) $\Sigma57$ and (112) $\Sigma35$ using Stllinger and Weber potential.[11] They reported that GB energies of these four GB's were in the close range of 1300–1370 mJ m^{-2}. The

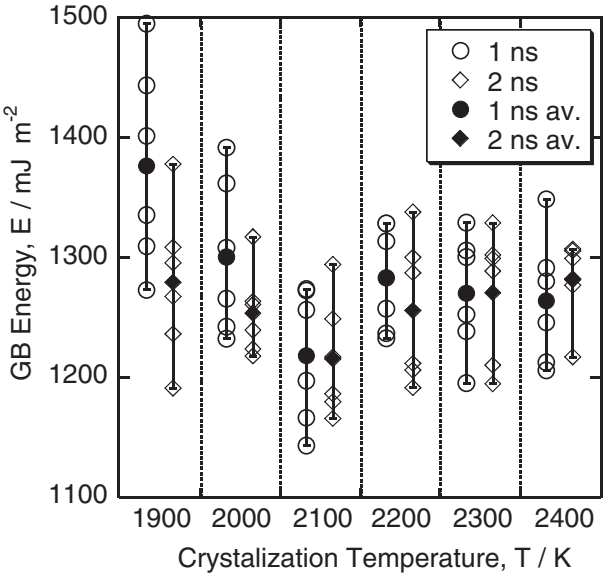

Fig. 4 GB energies obtained by the heat treatments of 1 and 2 ns crystallization are plotted at each crystallization temperature. The open symbols represent the calculated GB energies and closed symbols represent the average of six calculated GB energies. Details of the procedure is explained in the text.

average GB energy (1272 mJ m^{-2}) and the lowest GB energy (1143 mJ m^{-2}) in the present work were lower than the energies evaluated by Keblinski *et al.* The reason for this disagreement might arose from the difference of interatomic potentials. The period of the heat treatments applied in the present study was about seventeen times longer than that of Keblinski *et al.* Therefore, the structure of GB's simulated in the present work might be more stable than the structure simulated by them.

There have been only one experimental result for (010) twist boundaries in Si,[24] where GB energies were evaluated to be in the range of 450–500 mJ m^{-2} at 1473 K. Calculated GB energies with computer were rather large and showed a wide range of 1000–2500 mJ m^{-2}.[8,9] It is difficult to explain the difference between experimental values and calculated values. More experimental study for twist boundaries in Si is desirable.

3.4 GB structure

The GB's having the lowest and the highest GB energy (1143 and 1495 mJ m^{-2}) were chosen to examine the atomistic structure of the GB. A radial distribution function g(r) and a bond-angle distribution function P(cos θ) were calculated using atoms located within the estimated GB layer of 0.25 a_0 in thickness. The results are shown in Figs. 5(a) and (b), where g(r) and P(cos θ) of the amorphous Si are also shown for comparison. The amorphous Si was made by the heat treatment shown in Fig. 2 without introducing seed crystals. The atomistic structure of the calculated GB is roughly similar to that of the calculated amorphous Si.

The results of Keblinski *et al.*[9] discussed in the preceeding section showed that GB energies were reduced by melting and crystallization at high temperature because of the formation of an amorphous layers at the GB. The present results agree with their results.

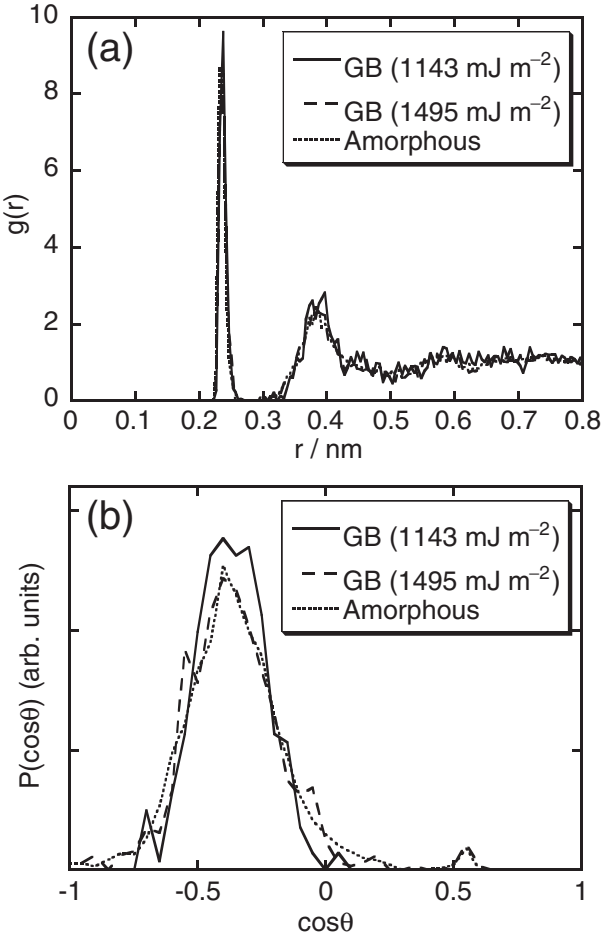

Fig. 5 The radial distribution function g(r); (a), and the bond angle distribution function P(cos θ); (b), for atoms within the estimated GB layer of 0.25 a_0 in thickness. The g(r) and P(cos θ) for the GB's having the lowest and the highest GB energy (1143 and 1495 mJ m^{-2}) are shown together with those for the amorphous Si.

3.5 Diffusion coefficients of atoms around GB's

In order to investigate the migration of atoms around GB's, the mean square displacement $\langle R^2(t)\rangle$ at 1900, 2000, 2100, 2200, 2300 and 2400 K were calculated by

$$\langle R^2(t)\rangle = \frac{1}{N_s N}\sum_{l=0}^{N_s-1}\sum_{i=1}^{N}[\boldsymbol{r}_i(t+t_0+l\Delta\tau) - \boldsymbol{r}_i(t_0+l\Delta\tau)]^2, \quad (3)$$

where N_s is the number of sampling, N is the number of atoms, $\boldsymbol{r}_i$ is the position of the atom i, t_0 is the start time of sampling and $\Delta\tau$ is the sampling interval. In the present study, N_s was 100, N was 2000, t_0 was 0.1 ns after the actual start time of the annealing at the above-mentioned temperature and $\Delta\tau$ was 0.1 ps.

In order to compare the mean square displacement of atoms around low and high energy GB's, two simulation cells (C1 and C2) were chosen to calculate $\langle R^2(t)\rangle$. The cell 1 (C1) had two GB's whose average GB energy was 1237 mJ m^{-2} and the cell 2 (C2) had two GB's whose average GB energy was 1469 mJ m^{-2}. Each one of two GB's in the cell was sandwiched by R2 and R3, as shown in Fig. 1(d). Atoms in R2 and R3 were fixed to prevent the parallel translation of the

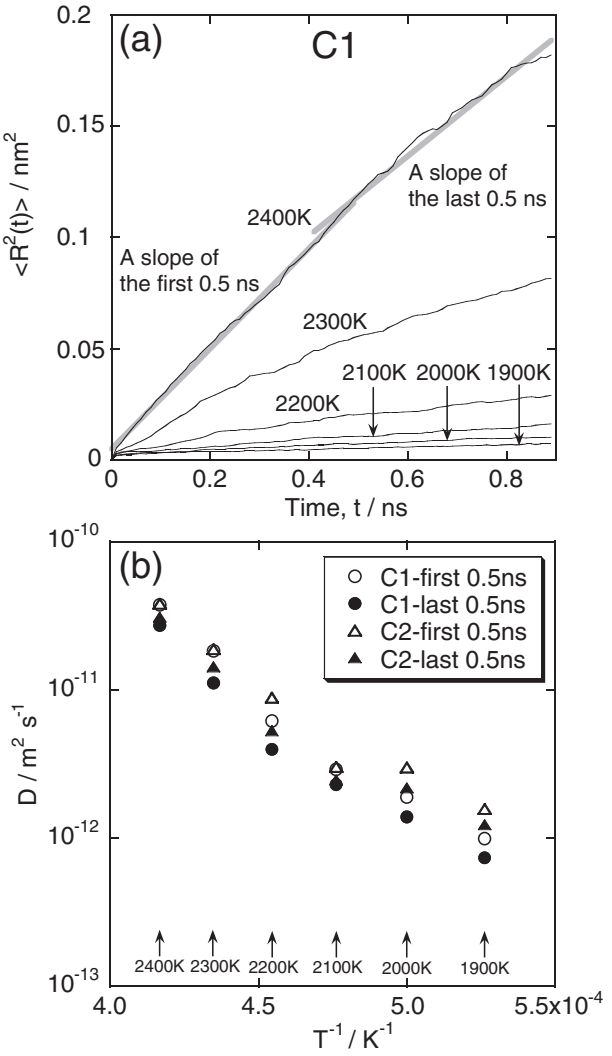

Fig. 6 (a) The mean square displacement $\langle R^2(t)\rangle$ for the simulation cell C1 of the low GB energy is shown against the annealing time. Two slopes used for evaluating diffusion coefficients are also indicated. (b) Diffusion coefficients D of atoms around GB's for the simulation cell C1 and the cell C2 of the high GB energy are shown against the reciprocal of the annealing temperature.

whole cell. Then the cell was heated again and kept at the above-mentioned temperature for 1 ns.

Figure 6(a) shows the results for the cell C1, and $\langle R^2(t)\rangle$ increased with time t. Atoms in the cell were checked by counting the number of neighbor atoms within the cut-off distance of Tersoff potential at the start and the end of each simulation, and vacancies and interstitials were not introduced in the crystalline part of the cell. Therefore, the increase in $\langle R^2(t)\rangle$ was attributed to the diffusion of atoms around two GB's.

The diffusion coefficient D was evaluated by

$$D = \langle R^2(t)\rangle/6t, \tag{4}$$

where the slope of $\langle R^2(t)\rangle/t$ was estimated by the least squares method. Since $\langle R^2(t)\rangle$ was slightly curved, two diffusion coefficients (C1-first 0.5 ns and C1-last 0.5 ns) at each temperature were evaluated using slopes within first 0.5 ns and within last 0.5 ns of the annealing time. Diffusion coefficients of C2-first 0.5 ns and C2-last 0.5 ns at each temperature were also evaluated for the cell C2 having high GB energy.

Table 1 The activation energies of atomic migration around GB's.

	Activation energy (eV)	
	1900–2100 K	2200–2400 K
C1-first 0.5 ns	1.9	4.1
C1-last 0.5 ns	2.0	4.4
C2-first 0.5 ns	1.1	3.3
C2-last 0.5 ns	1.2	4.0
Average	1.5	4.0

Figure 6(b) shows diffusion coefficients versus the reciprocal of temperature T. The activation energy E_a of atomic migration around GB's was evaluated by fitting the diffusion coefficients to the following equation,

$$D = D_0 \exp\left(-\frac{E_a}{kT}\right), \tag{5}$$

where D_0 is the diffusion constant and k is the Boltzmann constant. It was difficult to fit diffusion coefficients within all temperature range in Fig. 6(b) to eq. (5), and two different activation energies were evaluated for two different temperature ranges (1900–2100 K and 2200–2400 K). Table 1 shows the activation energies estimated for the two temperature ranges using the diffusion coefficients of C1-first 0.5 ns, C1-last 0.5 ns, C2-first 0.5 ns and C2-last 0.5 ns. The average activation energies for each temperature range are also shown in the table. Because the activation energies for two temperature ranges were clearly different, the diffusion process in each temperature range was explained as follows.

(1) Between 1900 and 2100 K, the thickness of the amorphous thin layer around GB was nearly constant during MD simulation, and atoms migrated in the amorphous thin layer. The activation energy for this process was about 1.5 eV.

(2) Between 2200 and 2400 K, expansion and shrinkage of the amorphous thin layer was raised in addition to the migration of atoms. The number of atoms contributing to the mean square displacement increased due to expansion of the amorphous thin layer, and the diffusion coefficient increased. Therefore, the activation energy was larger than that in the lower tamperature range. The activation energy for this process was about 4.0 eV.

Shin *et al.*[25] investigated the structural relaxiation dynamics in pure (unhydrogenated) amorphous silicon following ion-irradiation-induced defect injection by measuring the changes in electrical conductivity. They reported that the average activation barrier varied from 0.23 to 2.7 eV as a function of relaxiation state. These barriers should be lower when samples are far from equilibrium. These barriers should be higher in well-ralaxed samples, reaching values similar to those found in crystalline silicon. Self-diffusion in crystalline silicon has an activation energy of about 4.5 eV.[26] The activation energyies evaluated in the present work were in the range of these experimental values.

Table 2 MD simulations with carbon atoms.

No.	Initial position and arrangement of carbon atoms	Number of carbon atoms (atomic %)	Final grain orientation	Simulation time (ns)
1	R2-Clustered	3 (0.15)	R3	12.0
2	R2-Clustered	5 (0.25)	R3	4.9
3	R2-Clustered	5 (0.25)	R3	4.5
4	R2-Clustered	5 (0.25)	R2	12.1
5	R3-Clustered	5 (0.25)	R2	4.4
6	R3-Clustered	5 (0.25)	R2	9.2
7	R3-Clustered	5 (0.25)	R2	6.7
8	R2-Clustered	10 (0.5)	R3	3.8
9	R3-Clustered	10 (0.5)	R2	8.0
10	Random	5 (0.25)	R2+R3	10.0
11	Random	5 (0.25)	R2+R3	10.0
12	Random	5 (0.25)	R2+R3	10.0

3.6 Effect of carbon atoms on the GB migration

Carbon atoms were introduced in the cell to investigate effect of impurities during GB formation and GB migration. Twelve simulation was carried out changing initial position of carbon atoms, number of carbon atoms and random number sequence, as shown in Table 2. Figures 7(a), (b), (c) and (d) show the snapshots of the y-z projection of atoms during a MD simulation which correspond to No. 2 in Table 2. Fig. 7(a) show the original simulation cell that contains (010) Σ5 twist boundary and carbon atoms. Small gray spheres are silicon atoms and large black spheres are carbon atoms that make a cluster and are located in R2. R1 was first kept at 3500 K for 50 ps to make liquid phase and then R1 was quenched to crystallization temperature. Fig. 7(b) shows the cell that was kept at 2300 K for 1.0 ns. Nearly all the part of R1 was crystallized and a new GB was formed near the middle of R2 and R3. This result is same as the result without carbon atoms, which is shown in Fig. 1(c). The cell was subsequently kept at 2300 K, and then the GB on the left side of R2 moved to R2 at 4.0 ns, as shown in Fig. 7(c). Carbon atoms were segregated at the GB in this figure. These atoms prevented shrinkage of amorphous thin layer, and the GB never moved after that. Then the GB on the right side of R2 moved to R2 at 4.9 ns, and the cell became a single crystal that has the crystal orientation of R3. In other word, the grain that contained clusterd carbon atoms shrunk and disappeared. In simulations from No. 1 to No. 9 except No. 4 in Table 2, the grain that contains clustered carbon atoms shrunk and disappeared. Carbon atoms made contraction strain field when precipitating in the grain, and it is thought that this strain field was the driving force for GB migration.

Figures 8(a) and (b) show the snapshots of the y-z projection of atoms during a MD simulation which corresponds to No. 10 in Table 2. Figure 8(a) show the original simulation cell that contains (010) Σ5 twist boundary and carbon atoms. Small gray spheres are silicon atoms and large black spheres are carbon atoms that are randomly located. R1 was first kept at 3500 K for 50 ps to make liquid phase and then R1 was quenched to crystallization temperature. Nearly all the part of R1 was crystallized and a new GB was formed

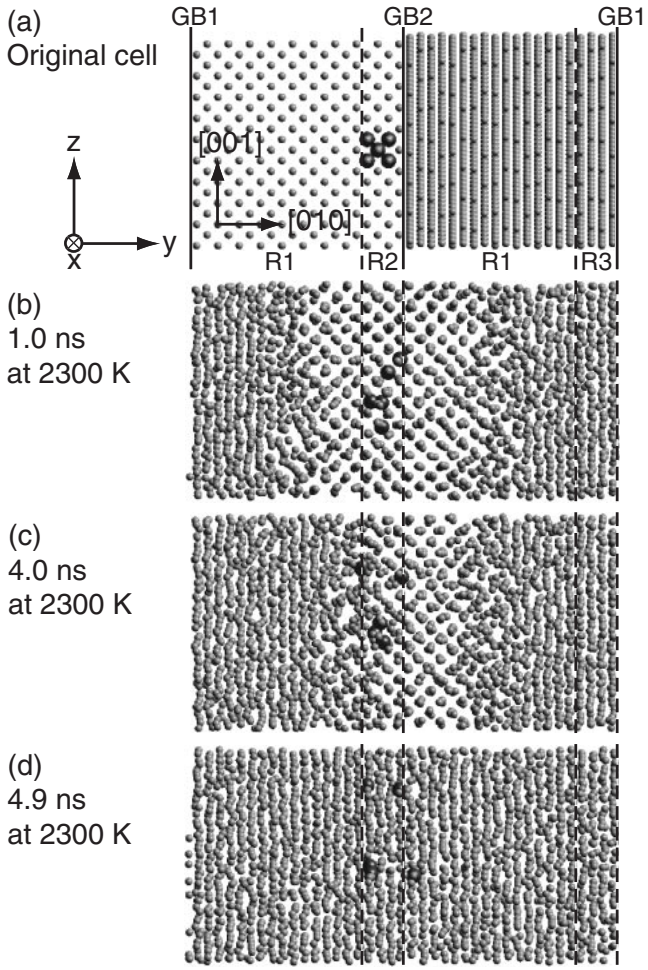

Fig. 7 Snapshots of the y-z projection of atoms during MD simulation including clusterd carbon atoms. (a) The original simulation cell contains (010) Σ5 twist boundary and carbon atoms. The right side crystal is made by rotating clockwise the left side crystal 36.9 degrees around the y-axis. GB1 and GB2 indicate grain boundaries, and details of R1, R2 and R3 are explained in the text. (b) After quench and 1 ns at 2300 K. (c) 4.0 ns at 2300 K. (d) 4.9 ns at 2300 K. Small gray spheres are silicon atoms, and large black spheres are carbon atoms.

near the middle of R2 and R3. Then the GB on the left side of R2 moved to left, and one carbon atom was segregated at the GB. Moreover, the GB on the right side of R2 moved to right, and two carbon atoms were segregated at the GB. These atoms prevented shrinkage of amorphous thin layer, and the GB never moved after that. Fig. 8(b) shows the cell that was kept at 2300 K for 9.9 ns, and GB's were located near carbon atoms. Same processes were observed in simulations of No. 11 and No. 12 in Table 2. These results suggest that one or two atoms can retard GB migration.

4. Conclusions

MD simulation using Tersoff potential was carried out to investigate the formation of a twist boundary during crystallization of silicon from the liquid-state. The atomistic processes of the GB migration have been also investigated. The results came to the following conclusions.

(1) The atomistic structure of the calculated twist boundary was similar to that of the calculated amorphous silicon,

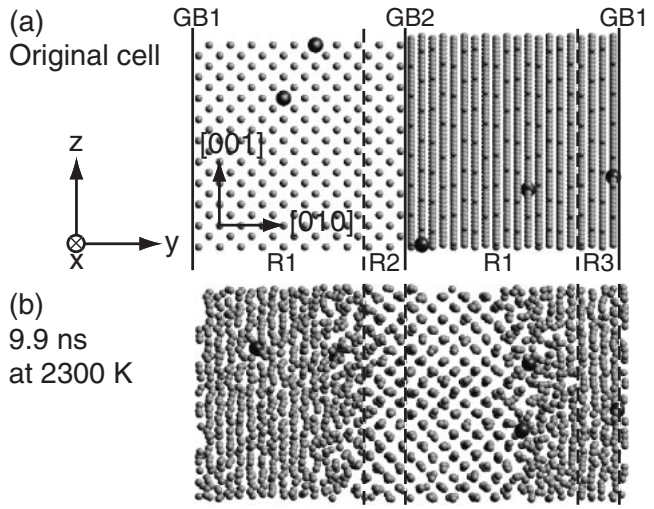

Fig. 8 Snapshots of the y-z projection of atoms during MD simulation including randomly located carbon atoms. (a) The original simulation cell contains (010) Σ5 twist boundary and carbon atoms. (b) 9.9 ns at 2300 K. Small gray spheres are silicon atoms, and large black spheres are carbon atoms.

suggesting an amorphous thin layer at the twist boundary.

(2) Changes in the thickness of an amorphous thin layer at the twist boundary was recognized after crystallization at temperatures higher than 2200 K (0.86 T_m). This atomistic process caused the GB migration.

(3) The activation energies of atomic migration around twist boundaries was 1.5 eV for the temperature between 1900 and 2100 K, and was 4.0 eV for the temperature between 2200 and 2400 K. Therefore, the diffusion mechanisms in each temperature range were different. The migration of atoms in the amorphous thin layer at twist boundaries was dominant at temperatures lower than 2100 K. Changes in the thickness of an amorphous thin layer was effective at temperatures higher than 2200 K in addition to the migration of atoms.

(4) When carbon atoms were segregated at a GB, these atoms prevented shrinkage of amorphous thin layer, and GB migration was retarded.

(5) Precipitated carbon atoms in a grain made contraction strain field, and this strain field became driving force for GB migration. The grain that contained carbon atoms shrunk, and the cell became a single crystal.

REFERENCES

1) M. J. McCann, K. R. Catchpole, K. J. Weber and A. W. Blackers: Sol. Energy Mater. Sol. Cells. **68** (2001) 135.
2) M. Miyasaka and J. Stoemenos: J. Appl. Phys. **86** (1999) 5556.
3) R. T. Howe, B. E. Boser and A. P. Pisano: Sensors and Actuators A **56** (1996) 167.
4) J. W. Tringe and J. D. Plummer: J. Appl. Phys. **87** (2000) 7913.
5) S. Christiansen, P. Lengsfeld, J. Krinke, M. Nerding, N. H. Nickel and H. P. Strunk: J. Appl. Phys. **89** (2001) 5448.
6) A. Voigt, E. Wolf and H. P. Strunk: Mat. Sci. Eng. B **54** (1998) 202.
7) M. Kohyama: Model. Simul. Mater. Sci. Eng. **10** (2002) R31.
8) M. Kohyama and R. Yamamoto: Phys. Rev. B **49** (1994) 17102.
9) P. Keblinski, S. R. Phillpot, D. Wolf and H. Gleiter: Phys. Rev. Lett. **77** (1996) 2965.
10) P. Keblinski, S. R. Phillpot, D. Wolf and H. Gleiter: Acta mater. **45** (1997) 987.
11) F. H. Stllinger and T. A. Weber: Phys. Rev. B **31** (1985) 5262.
12) R. W. Fancher, C. M. Watkins, M. G. Norton, D. F. Bahr and E. W. Osborne: J. Mater. Sci. **36** (2001) 5441.
13) M. I. Baskes: Phys. Rev. B **46** (1992) 2727.
14) J. Tersoff: Phys. Rev. B **37** (1988) 6991.
15) J. Tersoff: Phys. Rev. B **38** (1988) 9902.
16) J. Tersoff: Phys. Rev. B **39** (1989) 5566.
17) M. Ishimaru, S. Munetoh and T. Motooka: Phys. Rev. B **56** (1997) 15133.
18) M. Ishimaru, K. Yoshida, T. Kumamoto and T. Motooka: Phys. Rev. B **54** (1996) 4638.
19) T. Motooka, K. Nishihara, S. Munetoh, K. Moriguchi and A. Shintani: Phys. Rev. B **61** (2000) 8537.
20) R. Biswas and D. R. Hamann: Phys. Rev. B **34** (1986) 895.
21) E. Helfand: Bell Syst. Tech. J. **58** (1979) 2289.
22) W. H. Press, S. A. Teukolsky, W. T. Vetterling and B. P. Flannery: *Numerical Recipes in Fortran 77 Second Edition*, (Cambridge University Press, New York, 1992) p. 387.
23) S. J. Cook and P. Clancy: Phys. Rev. B **47** (1993) 7686.
24) A. Otsuki: Acta Mater. **49** (2001) 1737.
25) J. H. Shin and H. A. Atwater: Phys. Rev. B **48** (1993) 5964.
26) W. Frank, U. Gosele, H. Mehrer and A. Seeger: *Diffusion in Crystalline Solids*, ed. by G. E. Murch and A. Nowick, (Academic, New York, 1984).